Hindawi
Journal of Environmental and Public Health
Volume 2023, Article ID 9763022, 12 pages
https://doi.org/10.1155/2023/9763022

Research Article

Artificial Neural Networks and Genetic Algorithms: An Efficient Modeling and Optimization Methodology for Degradation of Atenolol Using Activated Persulfate with Ultrasound

Zeynab Moradmand,[1,2] **Bahare Dehdashti**,[1,2,3] **Farzaneh Mohammadi**,[1] **Nasrin Zahedi**,[1,2] **Maryam Razaghi**,[1,2] **and Mohammad Mehdi Amin**[1,3]

[1]*Department of Environmental Health Engineering, School of Health, Isfahan University of Medical Sciences, Isfahan, Iran*
[2]*Student Research Committee, School of Health, Isfahan University of Medical Sciences, Isfahan, Iran*
[3]*Environment Research Center, Research Institute for Primordial Prevention of Non-Communicable Disease, Isfahan University of Medical Sciences, Isfahan, Iran*

Correspondence should be addressed to Bahare Dehdashti; baharehdehdashty@yahoo.com and Mohammad Mehdi Amin; mohammadmehdia@gmail.com

Received 7 January 2023; Revised 15 March 2023; Accepted 28 March 2023; Published 20 June 2023

Academic Editor: Mahmoud Nasr

Atenolol (ATN) is a slowly biodegradable antagonist β-blocker drug and remains in the environment for a long period of time. This drug has a harmful effect on the environment and human and animal bodies. In this study, using activated persulfate with ultrasound for the degradation of ATN was investigated. The effect of independent variables including pH, ATN concentration, persulfate dose, contact time, and ultrasonic power has been studied at 5 levels. Central composite design (CCD) was used for designing the experiments in Design Expert 11.0 software. The ATN concentration was measured using high-performance liquid chromatography (HPLC). Genetic algorithms (GA) and artificial neural network (ANN) were used for optimization and prediction, respectively. The results indicated that at the optimal conditions for the experiment (pH of 6.79, reaction time of 19 min, initial ATN concentration of 15.92 mg/L, US power of 109.56 W, and PS dose of 1317.88 mg/L), the highest ATN degradation efficiency was 98.9%. The ATN degradation could be represented by the pseudo-zero-order kinetics. Also, the data of ATN were well fitted with the ANN model ($R^2 = 0.98$). The results showed that the best pH range to eliminate ATN is the near neutral range and the GA was found to be an effective tool to optimize the experimental conditions for the removal of ATN. The ultrasonic/persulfate process as a useful technique has a high potential to remove ATN from aqueous solutions.

1. Introduction

In recent decades, a group of emerging pollutants, pharmaceutical and personal care products (PPCPs), and medical compounds, due to worldwide use and complex sustainable structures, are one of the major environmental problems, which have attracted increasing attention [1, 2].

Atenolol (ATN) is a representative PPCP compound and one kind of the most prescribed antagonist β-blocker drugs that has been used for nearly 40 years, commonly used to treat hypertension, arrhythmia, glaucoma, and angina, and against coronary heart diseases [1, 3, 4].

This beta-blocker drug is resistant to natural attenuation and also biodegrades very slowly. Therefore, it enters surface

and ground waters and finally remains in the environment for a long period of time. This drug has also harmful consequences in animals and aquatic organisms such as the effect on heart rates and behavioral disorders in some invertebrates and vertebrates [2, 5].

ATN has also been shown to inhibit the growth of embryonic cells and can also affect the level of testosterone in humans by affecting the endocrine glands [1, 6].

Studies have shown that the toxicity of ATN to aquatic organisms and humans is the most serious among other b-blockers, and temperature affects the rate of degradation of ATN, indicating higher stability at 4°C. Furthermore, oral doses of ATN are excreted mostly (about 90%) unaltered through urine because it is not fully metabolized by the human body [7–9].

ATN extensively exists in a variety of aqueous environments, such as hospital wastewater, groundwater, and surface water [2, 6]. According to previous studies, conventional wastewater treatment plants (WWTPs) cannot remove β-blockers effectively, so beta-blockers in WWTP are often easily discharged into surrounding rivers and lakes. For this reason, more efficient and advanced water treatment processes are needed to remove these compounds [5].

New and additional processes such as advanced oxidation [10], reverse osmosis [11], activated carbon [12, 13], and membrane filtration [14] have been used for industrial wastewater treatment [15].

Advanced oxidation processes (AOPs) are generally defined as oxidation methods and in the last decade have received special attention due to being economical and having high efficiency. AOPs are primarily based on producing high oxidizing radicals such as OH•, O•, and SO_4• that can remove a large range of organic pollutants [16, 17].

Key AOPs known as produce active radical processes include the use of strong oxidizing agents such as hydrogen peroxide (H_2O_2), ozone (O_3), Fenton, photo-Fenton, photocatalysts (iron ions, electrodes, and metal oxides), radiation (UV light, sunlight, and ultrasound), and electrochemical oxidation that alone or in combination are effective in eliminating volatile organic matters and odor control [18, 19].

Among the various AOPs, ultrasound (US) is more popular for wastewater treatment due to the lack of production of intermediate pollutants, the activation of persulfate ion, and production of free radicals [20].

US treatment, which produces radical hydroxyl and oxygen due to microbubbles through the cavitation phenomenon in the solution, is an efficient method for destroying organic pollutants [20, 21].

Persulfate (PS) has desirable properties including easy storage and transportation, high stability, rapid reaction, and cost-effectiveness, and it is one of the strongest oxidants compared to others.

The production of sulfate radicals and subsequent hydroxyl radicals by persulfate is shown in the following equation [22]:

$$SO_4^{0-} + H_2 \longrightarrow OH^0 + HSO_4^- \quad (1)$$

Advanced design of experiments (DOE) techniques help us better understand and optimize the response. There are two main types of experimental designs, including central composite designs and Box–Behnken designs. A central composite design is the most commonly used design of experiments method. Central composite designs are a factorial or fractional factorial design with center points, augmented with a group of axial points (also called star points) that let you estimate curvature and nonlinear relationships. CCD is a more useful methodology for modeling various technological processes in the case of small number of preformed experiments compared with "one variable at a time" approach [23].

Today, one of the essential stages in the advanced oxidation processes is to model and optimize the parameters those are efficient in the process [24]. Nowadays, one of the most significant prediction and optimization methods is the use of artificial intelligent models and evolutionary algorithms, such as artificial neural networks (ANNs) and genetic algorithm (GA), which have been applied in many studies [25].

ANNs are very efficient tools for nonlinear statistical data modeling because they use learning algorithms that can independently make predictions as they receive new input [26]. GA is a method for optimization and solving problems based on a natural selection process that imitates biological evolution [27]. This method could be applied to solve problems that are not well suited for standard optimization algorithms, including problems in which the objective function is stochastic, nondifferentiable, highly nonlinear, or discontinuous [25].

Considering the adverse effects of atenolol and its impact on human health, the aim of this study was to remove ATN using a persulfate/ultrasonic process as an effective, simple, and environmentally friendly method. In addition, the effect of five quantitative effective variables including persulfate concentration, ultrasonic power, initial concentration of ATN, pH, and reaction time on the ATN removal efficiencies was evaluated. Also, the experimental data were modeled and optimized through ANN and GA, respectively. In addition, to the best of the authors' knowledge, this type of analysis for ATN has been reported in no previous literature.

2. Materials and Methods

2.1. Materials. In this study, atenolol ($C_{14}H_{22}N_2O_3 \geq 98\%$) was purchased from Raha Company (Iran). Ammonium persulfate ($(NH_4)_2S_2O_8$), potassium dihydrogen phosphate (KH_2PO_4), chlorine (Cl), nitrate (NO_3^-), and humic acid ($C_9H_9NO_6$) were supplied from Sigma-Aldrich (USA). Acetonitrile (HPLC grade; $C_2H_3N \geq 99\%$) and ethanol (HPLC grade; $C_2H_5OH \geq 99/9\%$) were purchased from Merck Co. (Germany). Hydrochloric acid (HCl) and sodium hydroxide (NaOH) were used to adjust the pH. All of the materials were of analytical grade and used as received without further purification. The deionized water was used to dilute the aqueous solutions.

2.2. Experimental Procedure. The present descriptive-analytical study is an experimental intervention that is performed as a laboratory scale batch reactor to remove ATN from aqueous solutions using the process of activating persulfate by ultrasonic on synthetic samples. In this research, five independent variables including pH (3, 5, 7, 9, and 11), ATN concentration (1, 5, 10, 15, and 20 mg/L), persulfate does (100, 250, 500, 1000, and 2000 mg/L), contact time (5, 10, 15, 20, and 30 min), and ultrasonic power (30, 60, 90, 120, and 150 W) were studied.

2.3. Analytical Methods. The concentration of ATN in samples was determined by using high-performance liquid chromatography (HPLC), Waters Company (USA), with a UV-2075 detector at 231 nm and C18 column. The mobile phase was acetonitrile/potassium dihydrogen phosphate with 70/30 (v/v) ratio at the flow rate of 1 mL/min. 20 μL of the sample was injected while the column temperature was set at 25°C. The removal efficiency of ATN was calculated according to the following equation:

$$\mathrm{R}\,\% = \frac{C_0 - C_e}{C_0}\,100, \tag{2}$$

where C_0 is the initial ATN concentrations in the solution (mg/L) and C_e is equilibrium ATN concentrations after degradation (mg/L).

An ultrasonic homogenizer (Bandelin-UW 3200, Germany) was used to produce ultrasonic waves for the degradation of the experiments. The specifications of the ultrasonic device used in this study are given in Table 1.

2.4. Design of Experiments. In this research, the CCD was applied for the design of the experiments, using Design Expert 11.0 software, considering 5 levels for each variable. Finally, a matrix with 32 runs was suggested by the software for this study. The suggestion of the software for the number of experiments was based on 16 cube points, 6 center points in cube, and 10 axial points. Table 2 shows the variables and levels considered.

2.5. Kinetics Analysis. The study of the degradation kinetics of atenolol was performed under the optimum condition. The effect of scavenger pollutions, chloride, nitrate, and humic acid on ATN degradation was also investigated. The analysis of humic acid content was performed using UV adsorption at 254 nm. Chloride and nitrate ions were also quantified [28].

2.6. Modeling and Optimization Details

2.6.1. Artificial Neural Network. The ANN was used to determine nonlinear relations between variables. MATLAB software R2017a version was used with the neural network toolbox (nnool) for the ANN modeling. A three-layer feedforward backpropagation neural network was developed by applying the tangent sigmoid (tansig) and linear (purlin) transfer functions in hidden and output layers, respectively, with the Levenberg–Marquardt training algorithm. The ANN model comprised five input parameters which include initial concentration, pH, PS, US, and time. The output layer was composed of one neuron representing removal efficiency. The 32 obtained samples were randomly divided into three categories including training (70%), validation (15%), and test (15%) subsets.

Table 1: Ultrasonic device specifications used in this study.

Specifications	Description
Frequency	20 KHz
Power	50–150 W
Voltage	230 (±10) V
Sample volume (batch)	0.5–1000 mL

Table 2: Experimental levels of independent process variables.

Factor	Name	Units	Min	Max	Levels
A	ATN	mg/L	1.00	20.00	1, 5, 10, 15, 20
B	PS	mg/L	100.00	2000.00	100, 250, 500, 1000,2000
C	US	W	30.00	150.00	30, 60, 90, 120, 150
D	*t*	Min	5.00	30.00	5, 10, 15, 20, 30
E	pH	—	3.00	11.00	3, 5, 7, 9, 11

The response of a neural network as well as the prevention of overfitting was significantly affected by the number of neurons in hidden layers, and thus, the number of neurons in the hidden layer was obtained by trial and error within the interface of the following equations:

$$\frac{2(i+o)}{3} < n_h < i(i+o) - 1, \tag{3}$$

$$\frac{n}{\alpha(i+o)} < n_h < \frac{n}{\alpha(i+o)}, \quad 1 < \alpha < 10, \tag{4}$$

where i, o, n, and n_h are the number of input neurons, output neurons, datasets, and the hidden layer neurons, respectively [29].

The accuracy of the optimized ANN model was calculated using the determination coefficient (R^2) and also the mean square errors (MSE) (equations (5) and (6)) [26]:

$$R^2 = \frac{\sum_{i=1}^{N}\left(y_i - yi_{-\mathrm{pred}}\right)^2}{\sum\left(y_{i-av} - y_{i-\mathrm{pred}}\right)^2}, \tag{5}$$

$$MSE = \left(\frac{1}{N}\right)\sum_{i=1}^{N}\left(yi - yi_{-\mathrm{pred}}\right)^2, \tag{6}$$

where y_i and $y_{i\text{-pred}}$ are the experimental and predicted values obtained from ANN, N is the number of experiences, and $y_{i\text{-av}}$ is the average of the experimental values.

2.6.2. Genetic Algorithm Optimization. The GA was implemented in the MATLAB software R2017a version. GA was used to determine the optimal conditions for ATN removal using the ANN model developed in this study as fitness function as follows: fitness function = Max (removal rate from ANN simulation).

Other settings intended for the genetic algorithm are number of generation 250, the rank scaling function, the selection function of Stochastic uniform, the number of elite 2, crossover fraction equal to 0.8, and the mutation function of constraint dependent and combination of scattered function [30].

3. Results and Discussion

3.1. Modeling with ANN. To determine the best neural network topology with the mentioned specifications, several networks with different numbers of hidden neurons were developed, and finally, the 5 : 5 : 1 topology showed the best performance.

Figure 1(a) shows the structure of a three-layer neural network that has five parameters in the input layer, five neurons in the hidden layer, and one parameter in the output layer.

Figure 1(b) represents the training, validation, and testing errors against the number of epochs (iterations) for the ANN models. Usually, the error decreases after some epochs of training and the training algorithm terminates if the validation error increases after six sequence iterations, or the limitations of the maximum error/epoch are exceeded. As demonstrated in Figure 1(b), the training algorithms for ANN are terminated in 2 epochs (because of the validation error), while the training errors are small enough. The test and validation error plots demonstrate similar characteristics. This is an indication of appropriately divided data in this study. The MSE values of the validation step are equal to 0.001044.

In Figure 1(c), the regression plots reveal the network outputs regarding targets for training, validation, and test groups. For a perfect fit, the data should fall along a 45-degree line, where the network outputs are equal to the targets. It is observed that the output tracks the targets very well for training (0.982), validation (0.999), and testing (0.968). Also, the coefficient of determination for the whole data was obtained 0.982. In this study, the network response is satisfactory and simulation could be used for entering new inputs. What is clear from the ANN results is that no overfitting has occurred in the developed network [31]. In Figure 1(d), a comparison diagram of the experimental and predicted results is presented.

3.2. The Effect of Influencing Variables on ATN Degradation. Using the designed neural network, the diagrams (Figure 2) were drawn in MATLAB software. The parameters shown inside each graph were considered variable, and the other parameters for each graph were fixed and equal to its optimal value (obtained from the genetic algorithm).

3.2.1. Effect of Initial Concentration of ATN. Figure 2(a) indicates that the initial concentration of ATN has a nonlinear correlation with the removal efficacy. The removal efficiency of ATN improved with an increase in the initial ATN concentration from 1 to 15 mg/L which shows the optimal concentration; then after that, increasing the concentration reduces the removal efficiency. In my opinion, when the initial concentration decreases in the solution, the number of ATN molecules among the water molecules is low and hidden between them, so ultrasonic waves have no significant effect on the ATN molecules and they reduce the removal efficiency.

On the other side, Aravindakumar et al. believed that increasing the initial concentration of ATN and also increasing the pH due to the recombination of OH• radicals and the existence of byproducts of ATN oxidation that compete with ATN molecules in the consumption of OH• cause a lack of OH• to react with atenolol and these factors reduce the removal efficiency [32].

Dehdashti et al. who studied on atenolol removal using multiwalled carbon nanotubes concluded that increasing the initial concentration of ATN has decreased the removal efficiency, and the reason is that increasing the initial concentrations of atenolol causes the rapid saturation of limited adsorption sites on an adsorbent [33].

Persulfate also had an almost nonlinear relationship. However, at a higher persulfate concentration, higher removal efficacy was obtained. It may be because $OH^{\bullet}$ radicals' formation is almost steady on the higher dose of PS and that they become the restricting reactants. Moreover, the presence of further quantity of SO_4^{-} gives higher degrees of oxidizing species. However, on the other hand, large amounts of PS have a negative effect on ATN degradation efficiency and show an inhibition effect because SO_4^{-} radicals react with themselves and produce S_2O_8 as shown in the following equation [34]:

$$S_2O_8^{2-} + SO_4^{-} \longrightarrow SO_4^{2-} + S_2O_8^{-} \quad (7)$$

A recent study on ATN removal by heat-activated persulfate found the same results. It says that the ATN degradation rates well followed pseudo-first-order kinetics under different PS dosages [35].

3.2.2. Effect of pH. The pH of solution is a significant factor that affects the type and amount of produced free radicals, and the rate of decomposition of target compounds in the advanced oxidation process is based on the persulfate [22]. The effect of different ranges of pH solution and ATN concentration on the degradation of ATN and other parameters which have been kept at optimal condition was studied in this research. Figure 2(b) shows nonlinear association between pH and the removal rate. As seen, with the rising of pH from 3 to 7 and also increasing of ATN concentration, the removal efficiency of ATN was increased to more than 90%. However, after this point, increasing pH and ATN concentration reduced the removal efficiency. The reaction of activated sulfate with ultrasonic waves was investigated in 3 ranges of acidic ($pH < 7$), neutral ($pH = 7$), and alkaline ($pH > 7$). In each range, some reactions occur and radicals are produced that affect the mechanism of PS oxidation.

Salehi et al. conducted a study on advanced oxidation which showed that in acidic pH, the oxidation efficiency increased within the $UV/K_2S_2O_8$ process so that with decrease in the pH, persulfate is decomposed into sulfate free radicals and can be further catalyzed by acid (equations (8) and (9)) [36]:

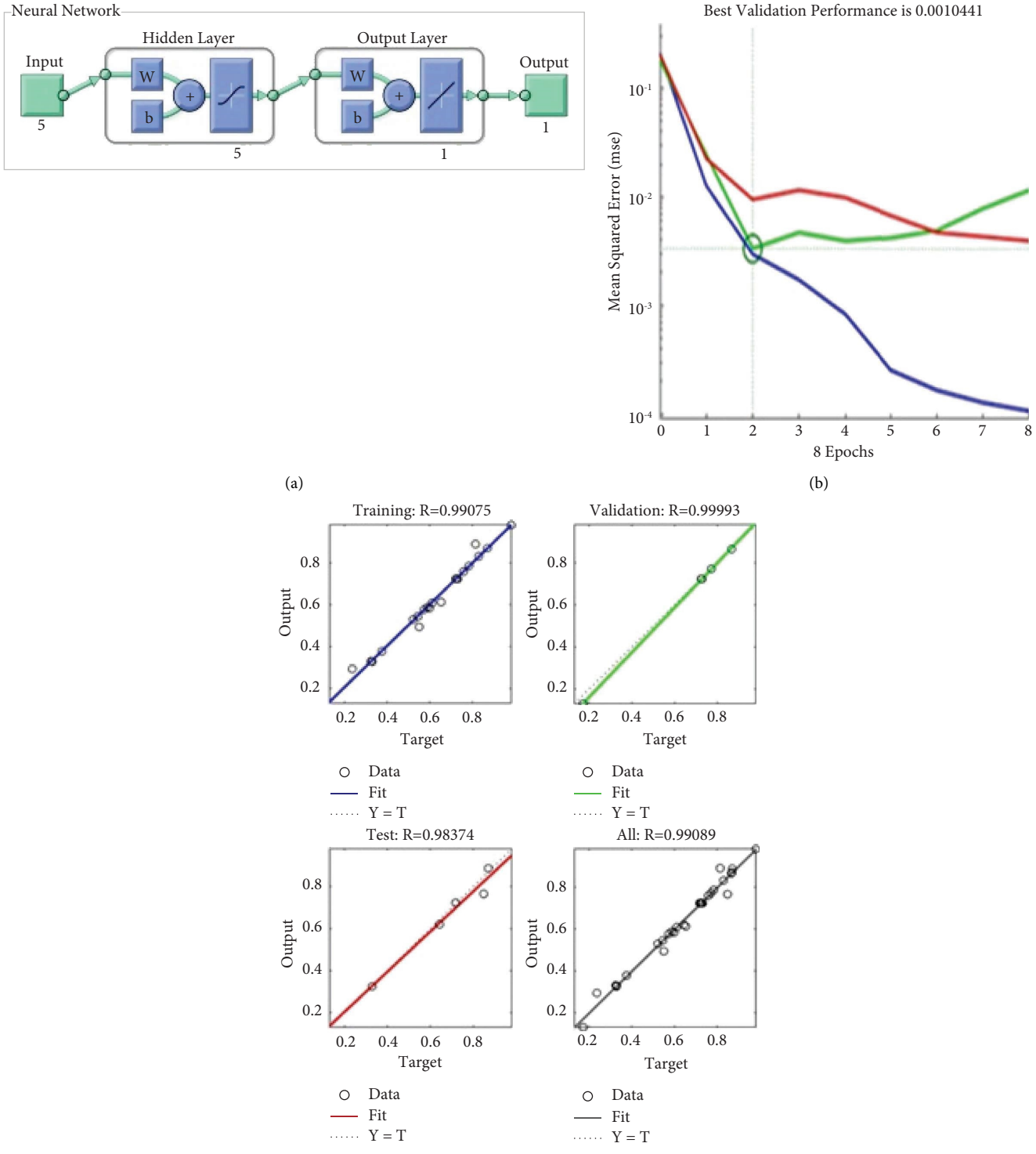

Figure 1: Continued.

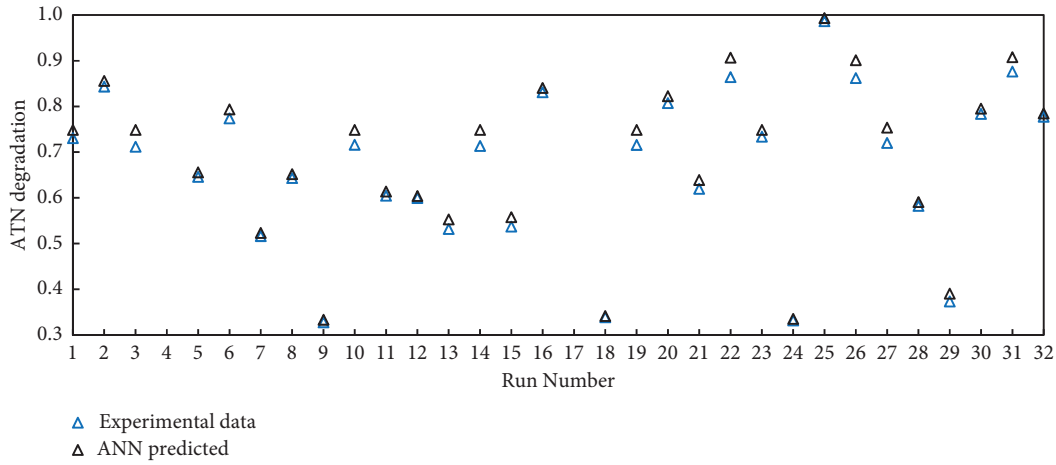

(d)

Figure 1: (a) Developed ANN structure, (b) validation performance, (c) regression plots of training, validation, and target for degradation efficiency of ATN, and (d) comparison of experimental and predicted.

$$S_2O_8^{2-} + H^+ \longrightarrow HS_2O_8^- \quad (8)$$

$$HS_2O_8^{2-} \longrightarrow SO_4^- + SO_4^{2-} + H^+ \quad (9)$$

In a study conducted by Harati and Rezaei Kalantary, when the pH is in the neutral range (pH = 7), hydroxyl radicals are produced which perform higher oxidation due to their longer half-life than sulfate radicals (as shown in equations (10)–(12)). On the other hand, in these conditions, there are other adverse reactions that lead to the consumption of hydroxyl radicals in solution. In equations (13) and (14), sulfate radicals can enter the reactions selectively [37].

$$2OH^\bullet \longrightarrow H_2O_2 \quad (10)$$

$$OH^\bullet + H_2O \longrightarrow H_2O_2 \quad (11)$$

$$2H_2O^\bullet \longrightarrow H_2O_2 \quad (12)$$

$$SO_4^\bullet + H_2O \longrightarrow OH^\bullet + SO_4^{2-} \quad (13)$$

$$SO_4^\bullet + OH^- \longrightarrow OH^\bullet + SO_4 \quad (14)$$

The study of Gao et al. showed that the degradation rate of ATN was decreased in alkaline conditions due to the reaction among SO_4^- with H_2O/OH^- which can convert SO_4^- into OH^- [35].

3.2.3. Effect of Ultrasound Power. Another parameter with a considerable effect on the removal of ATN is ultrasonic waves. Figure 2(c) reveals the effect of different ultrasonic intensities (30–150 W) with different times (5–30 min) on ATN degradation. The results showed that US has a direct association with the elimination efficacy and increasing US to 150 W leads to an increase in the removal efficiency up more than 95% and the effect of time is linear. According to equation (15), increasing the ultrasonic waves converts the sulfate anion into a sulfate radical which is responsible for the degradation of organic matter in an acidic environment, thus increasing the degradation of atenolol [17, 20].

$$S_2O_8^{2-} + US \longrightarrow 2SO_4^\cdot \quad (15)$$

Ultrasonic waves can also produce hydroxyl radicals according to equations (16)–(18):

$$H_2O + US \longrightarrow OH^\cdot + H^\cdot \quad (16)$$

$$OH^\cdot + OH^\cdot \longrightarrow H_2O_2 \quad (17)$$

$$H_2O_2 + e^- \longrightarrow OH^- + OH^\cdot \quad (18)$$

Razmi et al. studied the optimization of phenol removal from wastewater by activation of persulfate and ultrasonic waves in the presence of biochar catalyst modified by lanthanum chloride. Ultrasonic waves cause the formation and breakage of gas bubbles and produce hydroxyl radicals and hydrogen that can react with phenol and lead to its breakdown [38].

The study of Liu et al. on the removal of ketoprofen from water by sono-activated persulfate oxidation shows that greater ultrasonic power input can also produce more reactive radicals in the US/PS system. It was the same as findings of this study [21].

3.2.4. Effect of Contact Time. Another factor influencing the speed of reactions is contact time. Figure 2(d) shows the time versus the pH in ATN degradation. The effect of free radicals on ATN is reduced by the formation of compounds resulting from the breakdown of ATN. On the other hand, at lower contact time due to the lack of maximum formation of free radicals by ultrasonic waves and also the participation and use of the radical sulfate made in the process at the initial time, the efficiency is less than the optimal state [39].

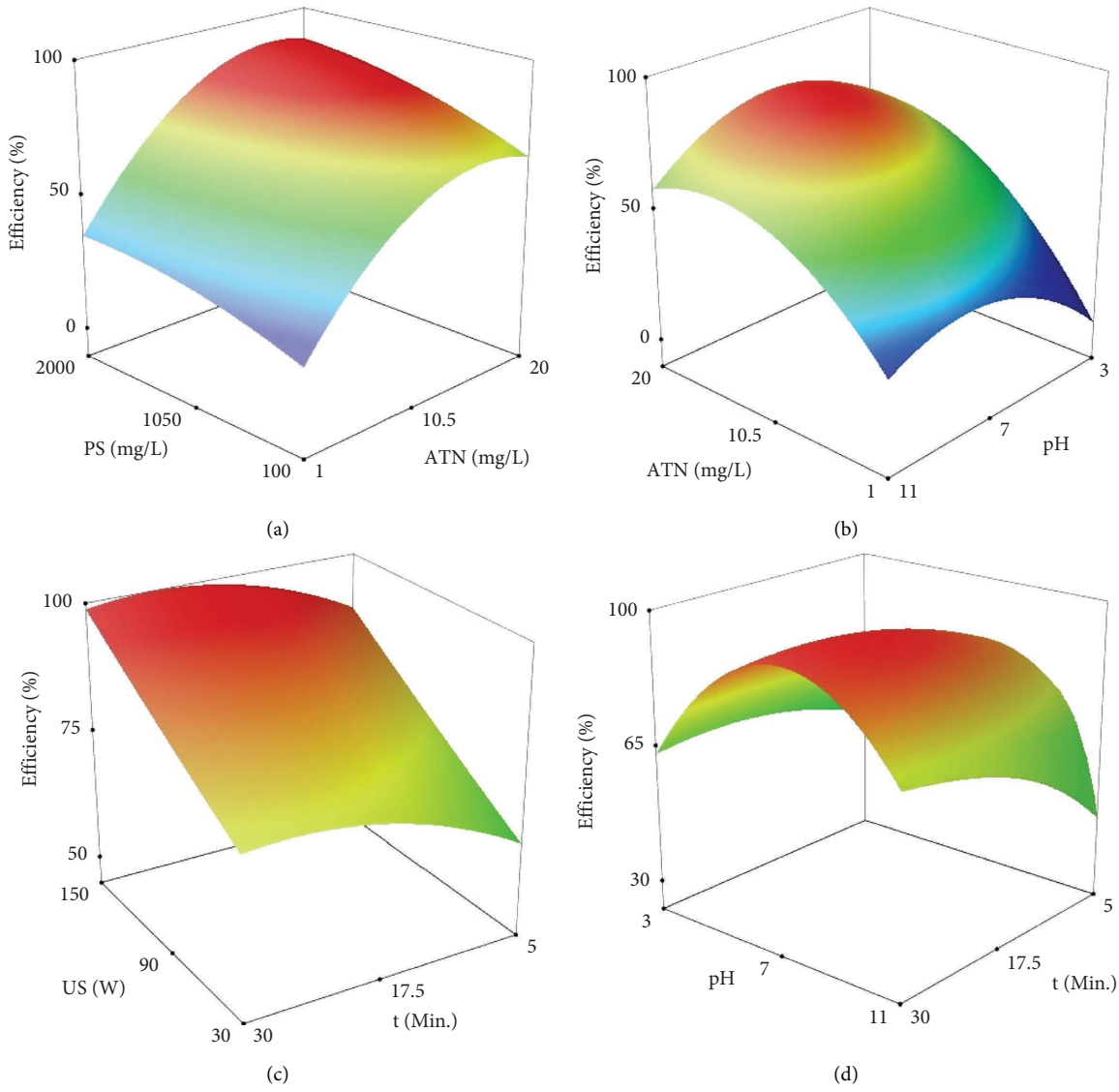

Figure 2: ANN prediction of the removal rate in different input parameters.

Movahedian Attar et al. reported similar results to our study that the optimum conditions were obtained at 17.5–18.5 mg/L and 60–65 min for 4-chlorophenol concentration and contact time, respectively, with the removal rate of 85.74%. However, by increasing contact time and 4-chlorophenol concentration, the removal efficiency has been declined. It could be because when the contact time increases more than the optimal time, it prevents hydroxyl radical accumulation because self-scavenging reaction may occur by nonradicals with persulfate. It says that the ATN degradation rates well followed pseudo-first-order kinetics under different PS dosage anions [22].

Dehdashti et al. in the study on using multiwalled carbon nanotubes for ATN removal showed that with extension of contact time from 5 to 60 minutes, an increasing trend was observed in the adsorption process. Then, a downward trend occurred until 90 minutes. The reason could be the fast filling of adsorption active sites by the adsorbate at the initial times [40].

3.3. Degradation Kinetics Modeling of ATN. The study of kinetics is necessary to evaluate the degradation rate and behavior of ATN molecules as a function of reaction time. In Table 3, the equations of pseudo-zero-, pseudo-first-, and pseudo-second-order kinetic models used in this study are presented. Kinetic plots fitted to the results of ATN removal efficiency by ultrasonic/persulfate are shown in Figure 3. As the constant of the degradation rate (k) and the correlation coefficients (R^2) are shown in Table 4, degradation of ATN is described better by pseudo-zero-order ($R^2 > 0.9197$) than other kinetic models. Tian et al. studied about synergic effectiveness of US/PS on diesel hydrocarbons (DHC) degradation from soil. They have also concluded that the pseudo-zero-order is more suitable for DHC degradation [41]. However, Li et al. investigated the treatment of soil contaminated with total petroleum hydrocarbons (TPH) using activated persulfate oxidation, ultrasound, and heat. They revealed that the pseudo-second-order reaction better evaluates the degradation of the TPH process by activated PS [42].

Table 3: The kinetic equations in the present study.

Kinetic type	Kinetic equation	Integrated form	Equation number
Pseudo-zero-order	$r_c = dc/dt = -k_0$	$C_e - C_0 = -k_0 t$	(19)
Pseudo-first-order	$r_c = dc/dt = -k_1 C$	$\ln(Ce/C0) = -k_1 t$	(20)
Pseudo-second-order	$r_c = dc/dt = -k_2 C^2$	$(1/Ce) - (1/C0) = k_2 t$	(21)

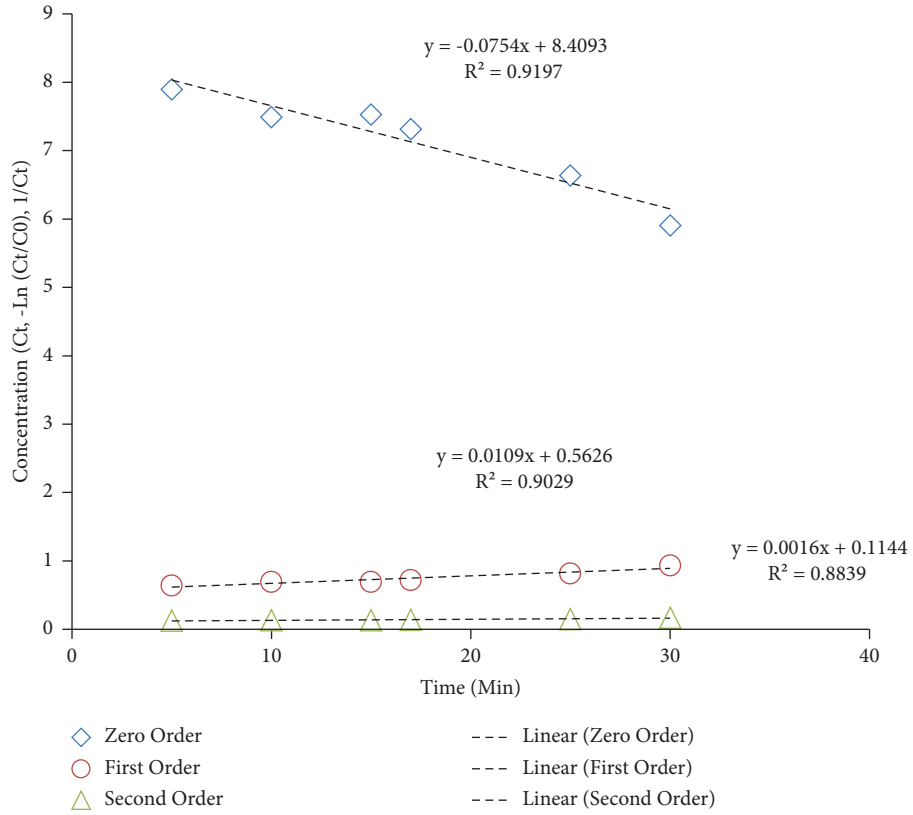

Figure 3: Kinetic fitted plots of ATN removal.

Table 4: Kinetic parameters of different models for ATN removal (pH: 6, initial ATN concentration: 15 mg/L, PS dose: 1317 mg/L, US power: 109 W, and reaction time: 19 min).

Model	K	R^2
Pseudo-zero-order	0.0754–	0.9197
Pseudo-first-order	0.0109	0.9029
Pseudo-second-order	0.0016	0.8839

3.4. Optimization with Genetic Algorithms. Figure 4(a) reveals the best and average fitness values in each generation. Figure 4(b) shows the best fitness values in the final generation. Hence, the optimal value of the input parameters, which are pH, time, US, PS, and ATN, was equal to 6.79, 19.0 min, 109.56 W, 1317.88 mg/L, and 15.92 mg/L, respectively. It leads to the highest removal efficiency of 98.92%. Table 5 compares the results of this study with some similar studies on removal efficiency. As can be seen in Table 5, there are various methods for removing pollutants from aqueous solutions. Some of the benefits of ultrasonication are safety, high efficiency, energy conservation, and cleanliness of the process [32]. Low ability to decompose organic matter at room temperature, cheapness, and high radical stability produced in different situations [17]. are the advantages of persulfate. Therefore, using ultrasonic/persulfate combination is more effective than other methods for ATN removal.

3.5. Sensitivity Analysis. Sensitivity analysis was conducted by the Pearson correlation method to evaluate which input independent parameter had the greatest effect on the removal efficiency. This analysis was performed separately for each of the input variables in a way that one input parameter was changed at equal intervals of a given point while the other input variables were kept constant [45].

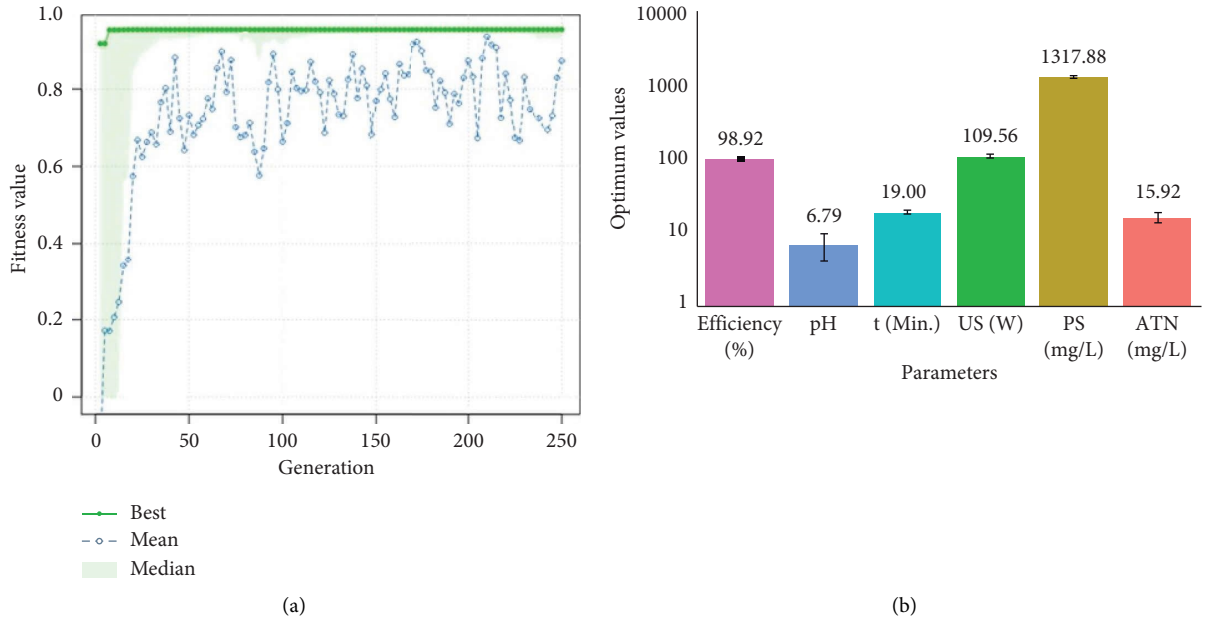

Figure 4: Genetic algorithm results: (a) the best and average fitness values per generation and (b) the optimal value of the input parameters and highest removal efficiency.

Table 5: Comparison of the results of this study with the findings of the similar research studies.

Pollutant	Degradation method	Optimum condition						References
		pH	Initial concentration of the pollutant (mg/L)	PS concentration (mg/L)	Time (min)	US power	Efficiency (%)	
4-Chlorophenol	Ultrasonic/Persulfate process	3	15	125	65	150	90.8	[22]
Atenolol	Sono-electro-persulfate process	7.4	11.2	200	18	—	99.8	[43]
Dimethyl phthalate	$UV_C/Na_2S_2O_8/Fe^{2+}$	11	5	0.514	90	—	95.7	[44]
Humic acid	Sono-persulphate process	3	—	—	39.29	—	74.75	[17]
Atenolol	Ultrasonic/persulfate process	6.8	15.9	1318	19	109.5	98.9	This study

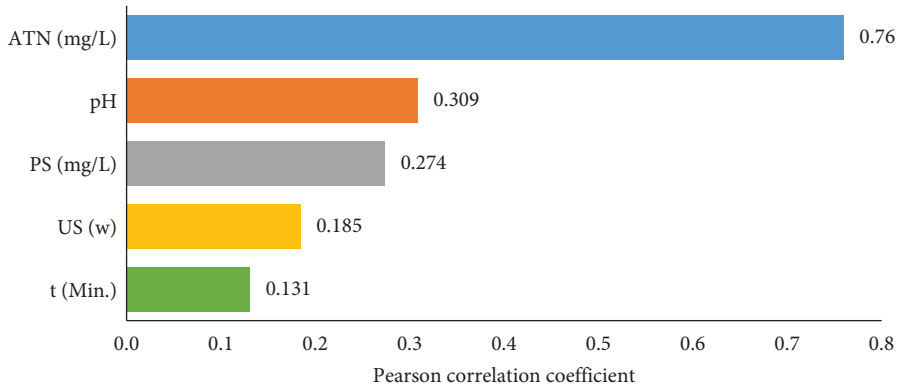

Figure 5: Sensitivity analysis using Pearson correlation.

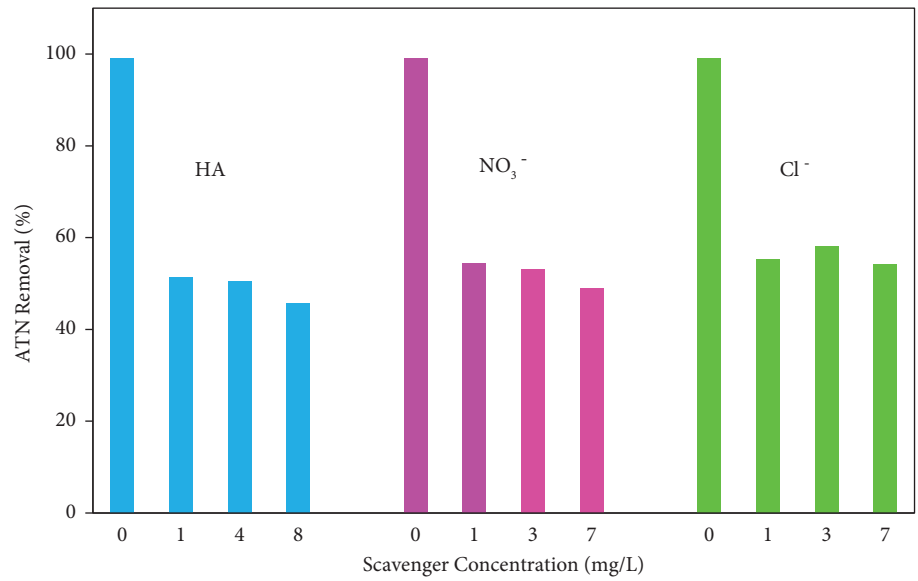

Figure 6: The effect of HA, NO_3^-, and Cl^- on ATN degradation by US activated PS (experimental condition: pH: 6, initial ATN concentration: 15 mg/L, PS dose: 1317 mg/L, US power: 109 W, and reaction time: 19 min).

Figure 5 indicates the comparison between the impacts of input parameters along with the coefficient effect of each parameter. According to Figure 5, the initial concentration of ATN with an impact factor of 0.76 is the most influential parameter on ATN removal and time has the least impact. The effect of the parameters is as follows: ATN > pH > PS > US > *t*.

3.6. Effect of HA, Nitrate, and Chloride on the Degradation of ATN. Nitrate (NO_3^-), chloride (Cl^-), and natural dissolved organic matter (NDOM) such as HA are widespread in ground or surface waters [46]. The presence of these materials is expected to interfere with the degradation of ATN by PS [35]. As shown in Figure 6, the degradation rate of ATN became slow with the presence of the scavengers. HA had the greatest effect among the scavengers, due to the fact that with increasing the concentration of HA from 0 to 8 mg/L, the degradation of atenolol decreased from 99% to 45.58%. As Lei et al. reported, inhibition of ATN degradation is related to competing between the ATN molecules and HA that during the reactions, HA binds to the OH^- and SO_4^{2-} free radicals and reduces the consumption of radicals by ATN [41]. Cl^- and NO_3^- are another materials and their inhibitory effects on different AOPs have been reported. Their mechanism of action in the restriction is the same as HA, but their impact is less than it [35, 46]. Liao et al. figured out that the inhibitory effects could be attributed to the consumption of free radicals (OH and SO_4^-) by Cl^- and formation of less reactive inorganic radicals [47]:

$$Cl^- + \dot{O}H \longrightarrow \dot{C}lOH^- \quad (19)$$

4. Conclusion

The results demonstrated that in the optimum condition of the ultrasonic/persulfate process, ATN removal of 98.92% was achieved. Degradation of ATN is described better by pseudo-zero-order ($R^2 > 0.9197$). ATN can be eliminated effectively at near neutral pH. The scavenging experiments confirmed that hydroxyl and sulfate radicals play a fundamental function in the degradation process. The outcomes confirmed that the background substances could have a negative impact on the elimination performance as $HA > Cl^- > NO_3^-$. The ANN model predicted the degradation efficiency with high accuracy (R^2: 98.2%).

Data Availability

The data generated and analyzed during this study are available from the corresponding author upon request.

Ethical Approval

The ethics code of this research is IR.MUI.RESEARCH.REC.1398.649.

Conflicts of Interest

The authors declare that they have no conflicts of interest.

Authors' Contributions

Zeynab Moradmand performed investigation and data curation and wrote the original draft. Bahare Dehdashti contributed to the concept, conducted the study, and wrote the original draft. Farzaneh Mohammadi was responsible for investigation, modeling, and revision of the manuscript.

Nasrin Zahedi performed investigation and revised the manuscript. Maryam Razaghi was responsible for conducting the study and revising the manuscript. Mohammad Mehdi Amin contributed to conceptualization, supervision, methodology, writing, reviewing, and editing.

Acknowledgments

This work was supported by the Isfahan University of Medical Sciences, research grant number: 198178.

References

[1] Z. Ran, L. Wang, Y. Fang, C. Ma, and S. Li, "Photocatalytic degradation of atenolol by TiO2 irradiated with an ultraviolet light emitting diode: performance, kinetics, and mechanism insights," *Catalysts*, vol. 9, no. 11, p. 876, 2019.

[2] J. Hu, X. Jing, L. Zhai, J. Guo, K. Lu, and L. Mao, "BiOCl facilitated photocatalytic degradation of atenolol from water: reaction kinetics, pathways and products," *Chemosphere*, vol. 220, pp. 77–85, 2019.

[3] P.-H. Chang, W. T. Jiang, B. Sarkar, W. Wang, and Z. Li, "The triple mechanisms of atenolol adsorption on ca-montmorillonite: implication in pharmaceutical wastewater treatment," *Materials*, vol. 12, no. 18, p. 2858, 2019.

[4] M. M. Amin, N. Bagheri, F. Mohammadi, and B. Dehdashti, "Sensitivity analysis with the Monte Carlo method and prediction of atenolol removal using modified multiwalled carbon nanotubes based on the response surface method: isotherm and kinetics studies," *International Journal of Chemical Engineering*, vol. 2022, pp. 1–12, 2022.

[5] Y. Gao, N..J. Gao, and D. Yin, "Oxidation of β-blocker atenolol by a combination of UV light and chlorine: kinetics, degradation pathways and toxicity assessment," *Separation and Purification Technology*, vol. 231, Article ID 115927, 2020.

[6] B. Dehdashti, M. M. Amin, A. Gholizadeh, M. Miri, and L. Rafati, "Atenolol adsorption onto multi-walled carbon nanotubes modified by NaOCl and ultrasonic treatment; kinetic, isotherm, thermodynamic, and artificial neural network modeling," *Journal of Environmental Health Science and Engineering*, vol. 17, no. 1, pp. 281–293, 2019.

[7] R. Karaman, K. Dajani, and H. Hallak, "Computer-assisted design for atenolol prodrugs for the use in aqueous formulations," *Journal of Molecular Modeling*, vol. 18, no. 4, pp. 1523–1540, 2012.

[8] X. Liu, T. Zhang, Y. Zhou, L. Fang, and Y. Shao, "Degradation of atenolol by UV/peroxymonosulfate: kinetics, effect of operational parameters and mechanism," *Chemosphere*, vol. 93, no. 11, pp. 2717–2724, 2013.

[9] N. K. Haro, P. Del Vecchio, N. R. Marcilio, and L. A. Féris, "Removal of atenolol by adsorption–Study of kinetics and equilibrium," *Journal of Cleaner Production*, vol. 154, pp. 214–219, 2017.

[10] S. Veloutsou, E. Bizani, and K. Fytianos, "Photo-Fenton decomposition of β-blockers atenolol and metoprolol; study and optimization of system parameters and identification of intermediates," *Chemosphere*, vol. 107, pp. 180–186, 2014.

[11] A. Urtiaga, G. Pérez, R. Ibáñez, and I. Ortiz, "Removal of pharmaceuticals from a WWTP secondary effluent by ultrafiltration/reverse osmosis followed by electrochemical oxidation of the RO concentrate," *Desalination*, vol. 331, pp. 26–34, 2013.

[12] J. Sotelo, A. Rodriguez, S. Alvarez, and J. Garcia, "Modeling and elimination of atenolol on granular activated carbon in fixed bed column," *International Journal of Enviromental Research*, vol. 6, 2012.

[13] G. Asgari, A. Dargahi, and S. A. Mobarakian, "Equilibrium and synthetic equations for index removal of methylene blue using activated carbon from oak fruit bark," *Journal of Mazandaran University of Medical Sciences*, vol. 24, no. 121, pp. 172–187, 2015.

[14] V. Homem and L. Santos, "Degradation and removal methods of antibiotics from aqueous matrices–a review," *Journal of Environmental Management*, vol. 92, no. 10, pp. 2304–2347, 2011.

[15] B. Dehdashti, "Atenolol absorption by multi-wall carbon nanotubes from aqueous solutions," *Journal of Mazandaran University of Medical Sciences*, vol. 26, no. 144, pp. 152–170, 2017.

[16] K. Hasani, M. Moradi, S. A. Mokhtari, H. sadeghi, A. Dargahi, and M. Vosoughi, "Degradation of basic violet 16 dye by electro-activated persulfate process from aqueous solutions and toxicity assessment using microorganisms: determination of by-products, reaction kinetic and optimization using Box–Behnken design," *International Journal of Chemical Reactor Engineering*, vol. 19, no. 3, pp. 261–275, 2021.

[17] S. Alizadeh, H. Sadeghi, M. Vosoughi, A. Dargahi, and S. A. Mokhtari, "Removal of humic acid from aqueous media using Sono-Persulphate process: optimization and modelling with response surface methodology (RSM)," *International Journal of Environmental Analytical Chemistry*, vol. 102, no. 16, pp. 3707–3721, 2022.

[18] H. Zhang, X. Liu, C. Lin et al., "Peroxymonosulfate activation by hydroxylamine-drinking water treatment residuals for the degradation of atrazine," *Chemosphere*, vol. 224, pp. 689–697, 2019.

[19] A. Rahmani, A. Ansari, A. Seid-mohammadi, M. Leili, D. Nematollahi, and A. Shabanloo, "Bismuth-doped 3D carbon felt/PbO2 electrocatalyst for degradation of diuron herbicide and improvement of pesticide wastewater biodegradability," *Journal of Environmental Chemical Engineering*, vol. 11, no. 1, Article ID 109118, 2023.

[20] A. Hossein Panahi, A. Meshkinian, S. D. Ashrafi et al., "Survey of sono-activated persulfate process for treatment of real dairy wastewater," *International journal of Environmental Science and Technology*, vol. 17, no. 1, pp. 93–98, 2020.

[21] Y.-J. Liu, B. He, C. Y. Hu, and S. L. Lo, "Removal of ketoprofen from water by sono-activated persulfate oxidation," *Water, Air, and Soil Pollution*, vol. 231, no. 7, pp. 1–12, 2020.

[22] H. Movahedian Attar, M. Darvishmotevalli, and M. Moradnia, "Degradation of 4-chlorophenol from aqueous solution using ultrasound/persulphate: prediction by RSM," *International Journal of Environmental Analytical Chemistry*, vol. 102, no. 17, pp. 6030–6040, 2020.

[23] J. R. W. Giles, E. M. Mount, and F. Harold, "25-Design of experiments," *Extrusion*, pp. 291–308, William Andrew Publishing, Norwich, NY, USA, Second Edition, 2014.

[24] R. Pelalak, R. Alizadeh, E. Ghareshabani, and Z. Heidari, "Degradation of sulfonamide antibiotics using ozone-based advanced oxidation process: experimental, modeling, transformation mechanism and DFT study," *Science of the Total Environment*, vol. 734, Article ID 139446, 2020.

[25] A. Smaali, M. Berkani, F. Merouane et al., "Photocatalytic-persulfate-oxidation for diclofenac removal from aqueous solutions: modeling, optimization and biotoxicity test assessment," *Chemosphere*, vol. 266, Article ID 129158, 2021.

[26] M. Berkani, M. K. Bouchareb, M. Bouhelassa, and Y. Kadmi, "Photocatalytic degradation of industrial dye in semi-pilot scale prototype solar photoreactor: optimization and modeling using ANN and RSM based on Box–Wilson approach," *Topics in Catalysis*, vol. 63, no. 11-14, pp. 964–975, 2020.

[27] F. Mohammadi, M. R. Samaei, A. Azhdarpoor, H. Teiri, A. Badeenezhad, and S. Rostami, "Modelling and optimizing pyrene removal from the soil by phytoremediation using response surface methodology, artificial neural networks, and genetic algorithm," *Chemosphere*, vol. 237, Article ID 124486, 2019.

[28] APHA, *Standard Methods for the Examination of Water and Wastewater, 23rd edn, American Public Health Association (APHA)*, American Water Works Association (AWWA) and Water Environment Federation (WEF), Washington, DC, USA, 2017.

[29] F. Mohammadi, B. Bina, H. Karimi, S. Rahimi, and Z. Yavari, "Modeling and sensitivity analysis of the alkylphenols removal via moving bed biofilm reactor using artificial neural networks: comparison of levenberg marquardt and particle swarm optimization training algorithms," *Biochemical Engineering Journal*, vol. 161, Article ID 107685, 2020.

[30] M. Razzaghi, A. Karimi, Z. Ansari, and H. Aghdasinia, "Phenol removal by HRP/GOx/ZSM-5 from aqueous solution: artificial neural network simulation and genetic algorithms optimization," *Journal of the Taiwan Institute of Chemical Engineers*, vol. 89, pp. 1–14, 2018.

[31] A. K. Rathankumar, V. K. Vaithyanathan, K. Saikia, S. S. Anand, V. K. Vaidyanathan, and H. Cabana, "Effect of alkaline treatment on the removal of contaminants of emerging concern from municipal biosolids: modelling and optimization of process parameters using RSM and ANN coupled GA," *Chemosphere*, vol. 286, Article ID 131847, 2022.

[32] K. Nejumal, P. R. Manoj, U. K. Aravind, and C. T. Aravindakumar, "Sonochemical degradation of a pharmaceutical waste, atenolol, in aqueous medium," *Environmental Science and Pollution Research*, vol. 21, no. 6, pp. 4297–4308, 2014.

[33] M. M. Amin, B. Dehdashti, L. Rafati, H. R. Pourzamani, M. Mokhtari, and M. Khodadadi, "Removal of atenolol from aqueous solutions by multiwalled carbon nanotubes: isotherm study," *Desalination and Water Treatment*, vol. 133, pp. 212–219, 2018.

[34] H. Ding and J. Hu, "Degradation of ibuprofen by UVA-LED/TiO2/persulfate process: kinetics, mechanism, water matrix effects, intermediates and energy consumption," *Chemical Engineering Journal*, vol. 397, Article ID 125462, 2020.

[35] D. Miao, J. Peng, X. Zhou et al., "Oxidative degradation of atenolol by heat-activated persulfate: kinetics, degradation pathways and distribution of transformation intermediates," *Chemosphere*, vol. 207, pp. 174–182, 2018.

[36] H. Salehi, A. A. Ebrahimi, M. H. Ehrampoush et al., "Integration of photo-oxidation based on UV/Persulfate and adsorption processes for arsenic removal from aqueous solutions," *Groundwater for Sustainable Development*, vol. 10, Article ID 100338, 2020.

[37] M. Harati and R. RezaeiKalantary, "Evaluation of efficiency of persulfate activated with ultrasonic waves in phenanthrene degradation from soil environments by central composite design method," *Journal of Environmental Health Engineering*, vol. 5, no. 4, pp. 309–322, 2018.

[38] R. Razmi, M. Ardjmand, B. Ramavandi, and A. Heydarinasab, "Optimization of phenol removal from wastewater by activation of persulfate and ultrasonic waves in the presence of biochar catalyst modified by lanthanum chloride," *Water and Environment Journal*, vol. 33, no. 4, pp. 499–507, 2019.

[39] N. Yousefi, S. Pourfadakari, S. Esmaeili, and A. A. Babaei, "Mineralization of high saline petrochemical wastewater using Sonoelectro-activated persulfate: degradation mechanisms and reaction kinetics," *Microchemical Journal*, vol. 147, pp. 1075–1082, 2019.

[40] B. Dehdashti, M. M. Amin, H. Pourzamani, L. Rafati, and M. Mokhtari, "Removal of atenolol from aqueous solutions by multiwalled carbon nanotubes modified with ozone: kinetic and equilibrium study," *Water Science and Technology*, vol. 2017, no. 3, pp. 636–649, 2018.

[41] Y.-J. Lei, Y. Tian, C. Fang et al., "Insights into the oxidation kinetics and mechanism of diesel hydrocarbons by ultrasound activated persulfate in a soil system," *Chemical Engineering Journal*, vol. 378, Article ID 122253, 2019.

[42] Y.-T. Li, J. J. Zhang, Y. H. Li, J. L. Chen, and W. Y. Du, "Treatment of soil contaminated with petroleum hydrocarbons using activated persulfate oxidation, ultrasound, and heat: a kinetic and thermodynamic study," *Chemical Engineering Journal*, vol. 428, Article ID 131336, 2022.

[43] N. Zahedi, B. Dehdashti, F. Mohammadi, M. Razaghi, Z. Moradmand, and M. M. Amin, "Using sono-electro-persulfate process for atenolol removal from aqueous solutions: prediction and optimization with the ANFIS model and genetic algorithm," *International Journal of Chemical Engineering*, vol. 2022, Article ID 1812776, 11 pages, 2022.

[44] M. Y. Badi, A. Esrafili, H. Pasalari et al., "Degradation of dimethyl phthalate using persulfate activated by UV and ferrous ions: optimizing operational parameters mechanism and pathway," *Journal of Environmental Health Science and Engineering*, vol. 17, no. 2, pp. 685–700, 2019.

[45] A. Alver, E. Baştürk, Ş. Tulun, and İ. Şimşek, "Adaptive neuro-fuzzy inference system modeling of 2, 4-dichlorophenol adsorption on wood-based activated carbon," *Environmental Progress and Sustainable Energy*, vol. 39, no. 5, Article ID e13413, 2020.

[46] X. Liu, L. Fang, Y. Zhou, T. Zhang, and Y. Shao, "Comparison of UV/PDS and UV/H2O2 processes for the degradation of atenolol in water," *Journal of Environmental Sciences*, vol. 25, no. 8, pp. 1519–1528, 2013.

[47] C.-H. Liao, S.-F. Kang, and F.-A. Wu, "Hydroxyl radical scavenging role of chloride and bicarbonate ions in the H2O2/UV process," *Chemosphere*, vol. 44, no. 5, pp. 1193–1200, 2001.